We are IntechOpen, the world's leading publisher of Open Access books Built by scientists, for scientists

4,800
Open access books available

122,000
International authors and editors

135M
Downloads

Our authors are among the

154
Countries delivered to

TOP 1%
most cited scientists

12.2%
Contributors from top 500 universities

CLARIVATE ANALYTICS BOOK CITATION INDEX INDEXED

WEB OF SCIENCE™

Selection of our books indexed in the Book Citation Index in Web of Science™ Core Collection (BKCI)

Interested in publishing with us?
Contact book.department@intechopen.com

Numbers displayed above are based on latest data collected.
For more information visit www.intechopen.com

Chapter

On the Limits of Photocatalytic Water Splitting

Bahar Ipek and Deniz Uner

Abstract

The major drawbacks on the limited H_2 and O_2 evolution activities of one-step photocatalytic water splitting systems are given here with the emphasis on charge recombination, back-oxidation reactions, and mass transfer limitations. Suppression of these unwanted phenomena is shown to be possible with the usage of small crystal-sized photocatalysts with low defect concentrations, presence of phase junctions, selection of co-catalyst that would be active for H_2 evolution but inactive for O_2 reduction, coating of the co-catalyst or the whole photocatalyst with selectively permeable nanolayers, and usage of photocatalytic systems with high solid–liquid and liquid–gas surface areas. The mass transfer limitations are shown to be important especially in the liquid–gas interfaces for agitated and suspended systems with estimated H_2 transfer rates in the range of ~200–8000 μmol/h.

Keywords: hydrogen production, photocatalyst, water splitting, mass transfer, back-oxidation

1. Introduction

Hydrogen gas is one of the best alternatives to fossil fuels since it has a high gravimetric energy density (142 MJ/kg) and it produces zero carbon upon combustion. Hydrogen is also used as a major reactant in environmentally important reactions such as carbon dioxide hydrogenation to methanol [1] or ammonia production (Haber-Bosch reaction) [2]. For hydrogen to be used as a *clean* energy source, its production via renewable ways is of great importance. It is conventionally produced via steam reforming of methane and fossil fuels (energy intensive, ΔH^0_{rxn} = 206 kJ/mol, 700–1100°C [3]) and coal gasification, which results in significant amounts of carbon dioxide production. The renewable ways for carbon-free production include biological sources (microalgae and cyanobacteria) and electrolysis of water using wind energy and photovoltaic cells as electricity generation sources. In addition to the mentioned renewable ways, photocatalytic water splitting/oxidation is a promising alternative, in which solar energy is used as the driving force to split water molecules to hydrogen and oxygen on the surface of a catalyst. This renewable production method of hydrogen is advantageous over other renewable methods due to the free source of energy and lower cost of the photocatalysts when compared to that of photovoltaic cells or wind turbines. Solar-driven catalytic (photocatalytic) reactions are considered to be of fundamental importance to the catalysis community since the solar energy is inexhaustible; i.e., the solar energy absorbed by the lands and oceans on an hourly basis (432 EJ/h

or 120,000 TW [4]) is comparable to the Earth's yearly energy consumption (reaching 575 EJ/year or 18 TW in 2017). However, the solar-to-hydrogen energy conversion efficiency value for photocatalytic water splitting systems is much lower (targeted to be 10%, currently reaching 1% [5]) than that of photovoltaic-assisted electrolysis (reaching 30% [6]) due to the major drawbacks in the one-step photocatalytic water splitting systems. Herein, we firstly introduce photocatalytic water splitting systems and give the major developments in materials such as visible light utilization and corresponding H_2 and O_2 production activity values (in Section 2). Then in Section 3, we discuss the causes of the low efficiencies in photocatalytic water splitting systems and the recent approaches in preventing energy efficiency-lowering factors such as inefficient visible light utilization, charge recombination, back-oxidation reactions, and mass transfer limitations.

2. Photocatalysis and water splitting

The first report on water splitting via harvesting photon energy is authored by Fujishima and Honda using a photoelectrochemical cell with a TiO_2 photoelectrode [7]. Following this first report suggesting the oxidation of water molecule via photo-generated holes on TiO_2 surface with the aid of small electrical voltage, photocatalytic water splitting on powder photocatalyst particles is demonstrated by other authors in the late twentieth century [8–15]. Metal-loaded semiconductors (such as Pt/TiO_2) are described as "short-circuited photoelectrochemical cells" that provide both the oxidizing centers and the reduction centers on the same catalyst (see **Figure 1**) [16].

Photocatalytic reactions are initiated by absorption of light having an energy higher than (or equal to) the bandgap of the photocatalysts that consist of semi-conductor materials. This bandgap energy should be larger than 1.23 V for overall water oxidation reaction, for which the maximum of the valence band and the minimum of the conduction band should be located at proper potentials for the oxygen and hydrogen evolution reactions to occur. To illustrate, the minimum of

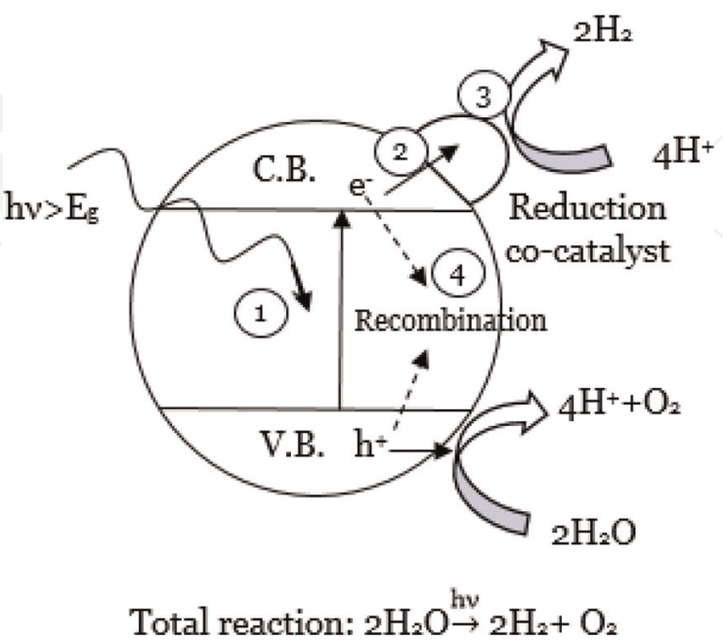

Figure 1.
Schematic representation of photocatalytic water splitting on metal-loaded semiconductor particle systems: (1) light absorption and charge excitation from valence band to conduction band, (2) transfer of the photo-generated electrons and holes to the catalyst surface, (3) surface redox reactions, and (4) charge recombination.

the conduction band energy level should be located at a more negative potential than 0 V vs. NHE, at pH = 0 for H_2 evolution (Eq. (1)), and the maximum of the valence band should be at a more positive potential than 1.23 V vs. NHE at pH = 0 for oxygen evolution reaction (Eq. (2)):

$$4H^+ + 4e^- \rightarrow 2H_2 \quad (1)$$

$$2H_2O + 4\,h^+ \rightarrow 4H^+ + O_2 \quad (2)$$

Following the light absorption, photoexcited electrons are transferred to the conduction band, while a positively charged charge carrier (hole) is generated at the valence band. These charge carriers are then transferred to the catalyst surface (step 2 in **Figure 1**) to be utilized in surface redox reactions, unless they recombine in the bulk or on the surface (step 4). Ultimately, electrons and holes reduce/oxidize the adsorbed species on the catalyst surface (step 3), the products of which should then be desorbed from the surface to complete the overall process.

2.1 Semiconductors

TiO_2, having a large bandgap (anatase: 3.2 eV), is the most commonly used photocatalyst due to its photostability, nontoxicity, and high activity (upon UV radiation $\lambda < 387$ nm). Following the report on water oxidation reaction [7], various photochemical reaction activities of TiO_2 such as carbon dioxide reduction with H_2O [17–19], alkene and alkyne hydrogenation [20, 21], CH_3Cl oxidation [22], 1-octanol degradation [23], phenol degradation [24], surfactant degradation [25], and more have been reported. Detailed reviews on TiO_2-based materials and photocatalytic performances can be found in literature [26–28].

As photostable and active TiO_2 is, UV light requirement to activate the large bandgap of TiO_2 motivated research for visible light active semiconductors as well as bandgap engineering for TiO_2 such as nonmetal ion doping (N [29], C [30], F [31], S [32]). Substitution of lattice oxygen atoms by these anions is reported to shift the valence band level upward and narrow the bandgap to as low as 2.25 eV (~550 nm) with 16.5% N doping [33].

Similar to TiO_2, oxides of other transition metals with d^0 (such as Ti^{4+}, Zr^{4+}, Nb^{5+}, Ta^{5+}, and W^{6+} [34, 35]) and d^{10} electronic configurations (such as Ga^{3+}, In^{3+}, Ge^{4+}, Sn^{4+}, and Sb^5 [36–38]) are shown to possess large bandgap energies (>3 eV) due to the maximum valence band levels consisting O_{2p} orbitals located near 3 V (vs. NHE at pH = 0). These d^0 and d^{10} metal oxide catalysts are reported to show remarkable one-step photocatalytic water splitting activity under UV light irradiation [39] reaching 71% quantum yield with photocatalysts such as Al-doped $SrTiO_3$ [40] or Zn-doped Ga_2O_3 [41]. The H_2 and O_2 evolution activity under UV radiation and the apparent quantum yields of some of these materials are given in **Table 1**. The apparent quantum yield is defined as the number of reacted electrons and holes divided by the number of incident photons on the photocatalysts. **Table 1** is not intended to cover the whole range of particulate catalysts in literature but rather to give a selection of examples. A wider selection of d^0 and d^{10} metal oxide particulate catalysts' one-step water oxidation activity and apparent quantum yields can be found in the works of Kudo et al., Chen et al., and Domen et al. [39, 42, 43].

The most remarkable upgrades in the apparent quantum yields are achieved by material engineering such as (i) doping the metal oxides/perovskites with cations having lower valences, (ii) decreasing the crystal sizes to submicron levels, and (iii) loading with H_2/O_2 evolution co-catalysts.

Semiconductor	Co-catalyst	Bandgap (eV)	H_2 activity (μmol/h)	O_2 activity (μmol/h)	AQY (%)	Reference
$La_2Ti_2O_7$:Ba	NiO_x	3.26	5000		50	[44]
$SrTiO_3$:Al	$Rh_{2-y}Cr_yO_3$	3.2	550*	280*	30 at 300 nm	[35]
$SrTiO_3$:Al (200–500 nm)	$Rh_{2-y}Cr_yO_3$	3.2	1372*	683*	56 at 365 nm	[45]
$SrTiO_3$:Al	$MoO_y/RhCrO_x$	3.2	1800*	900*	69 at 365 nm	[40]
$NaTaO_3$	NiO	4.0	3390	1580	20 at 270 nm	[46]
$NaTaO_3$:La	NiO	4.1	19,800	9700	56 at 270 nm	[34]
Ga_2O_3:Zn	NiO	4.4	4100	2200	20	[47]
Ga_2O_3:Zn	$Rh_{0.5}Cr_{1.5}O_3$	4.4	32,000	16,000	71 at 254 nm	[41]

**0.1 g of photocatalyst is used instead of 1 g.*

Table 1.
H_2 and O_2 evolution activity of d^0 and d^{10} metal oxide particulate catalysts under UV light irradiation.

2.2 Co-catalysts

An important addition to the light-harvesting semiconductors is H_2 evolution/O_2 evolution co-catalysts on the surface. The early co-catalysts that have been widely used included the noble metals and transition metal oxides such as Pt [12, 13], Rh [10], Ru [48], Au [49, 50], and NiO_x [11] that mainly promote the hydrogen evolution, and CoO_x [51] and Fe [52], Mn [52], RuO_2 [53], and IrO_2 [54] that accelerate the oxygen evolution. These metals are considered to act as charge carrier sinks that suppress electron–hole pair recombination as well as increasing the reaction kinetics by lowering the activation energy of the redox reactions. Co-catalysts are also known to inhibit photodegradation of the photocatalysts such as oxysulfides and oxynitrides by generated holes due to the effective extraction of these holes by the co-catalysts [55, 56].

Following the works of noble metal co-catalysts, Domen et al. showed water splitting activity on $SrTiO_3$ photocatalyst together with the co-catalyst NiO [57, 58], which became the choice of H_2 evolution co-catalyst for many d^0 and d^{10} metal oxides such as $La_2Ti_2O_7$:Ba [44], $La_4CaTi_5O_{17}$ [59], $Rb_4Nb_6O_{17}$ [60], $NaTaO_3$ [46], and Ga_2O_3:Zn [47]. The photocatalyst stability of NiO-loaded $K_2La_2Ti_3O_{10}$ is reported to increase by addition of a second co-catalyst, Cr, using a co-impregnation method [61]. Based on the promoting effect of Cr, a systematic study of Cr and various transition metals (such as Fe, Co, Ni, Cu, Ru, Rh, Pd, Ag, Pt) on $(Ga_{1-x}Zn_x)(N_{1-x}O_x)$ has been conducted [62], from which core-shell structures of core Rh nanoislands and shell Cr_2O_3 structures (10–30 nm in size) are found to promote H_2 and O_2 evolution reactions to significant levels [63].

2.3 Visible light utilization

The alterations to the semiconductors such as doping with low-valence cations, reducing particle sizes to submicron levels and obtaining a high degree of crystallinity help with the overall water splitting activity. However, activation of these photocatalysts uses a narrow portion of the solar spectrum (4%); i.e., the UV light sustains as a problem due to the large bandgap energies of these materials. To enable visible light utilization of the d^0- and d^{10}-type oxide semiconductors and to split water into H_2 and O_2 via one-step excitation, the valence band levels should be

shifted upward without changing the conduction band potentials. One approach to do this is to use oxynitrides to make use of N_{2p} states that lie at a more negative potential than O_{2p} states. Emerging $LaMgTa_{1-x}O_{1+3x}N_{2-3x}$ [64] and $Ga_{1-x}Zn_xN_{1-x}O_x$ [65] oxynitrides are representatives of visible light active overall water splitting catalysts. Using N doping, the absorbed light wavelength can be increased up to 500 nm on solid solutions of GaN:ZnO ($Ga_{1-x}Zn_xN_{1-x}O_x$) [66] and up to 600 nm on solid solutions of $LaTaON_2$ and $LaMg_{2/3}Ta_{1/3}O_3$ ($LaMgTa_{1-x}O_{1+3x}N_{2-3x}$) [64]. Other examples include $LaSc_xTa_{1-x}O_{1+2x}N_{2-2x}$ [67] and $CaTaO_2N$ [68] in which La or Ta sites are replaced by Ca and Sc that alters O/N ratios due to charge compensation, which in turn results in valence band energy level shift.

Some examples of visible light active photocatalyst and their H_2 and O_2 evolution activity are given in **Table 2**. As it can be seen from the table, one-step water splitting quantum yields are quite lower when compared to those of the UV-activated photocatalysts (**Table 1**). The exceptions to the low activity are reported by $Rh_{2-y}Cr_yO_3$ (Rh 1.0 wt%, Cr 1.5 wt%)-loaded $(Ga_{1-x}Zn_x)(N_{1-x}O_x)$ photocatalyst [63], multiband InGaN/GaN nanowire arrays [69], and monodisperse 4 nm graphite nanoparticle-deposited C_3N_4 catalysts [70].

An alternative way to cover both oxidation and reduction reactions with semiconductors that could be activated under visible light radiation is to utilize two individual photocatalysts with an electron transfer mediator to obtain two-step excitation known as the two-step water oxidation ("Z-scheme system," see **Figure 2**). In this system, O_2 evolution photocatalysts oxidize the water molecules to O_2, while the photo-generated electron is transferred to the mediator to reduce the electron acceptor (such as Fe^{3+} ions or IO_3^- ions). Then, the reduced mediator is oxidized by donating its electron to the H_2 evolution photocatalyst. At the same time, the photo-generated electrons in the H_2 evolution photocatalyst reduce H^+s to H_2.

The semiconductors used in this two-step water splitting process should be selected based on the energy levels of their corresponding valence or conduction band maximum/minimum that would enable O_2/H_2O oxidation and H^+/H_2 reduction. As H_2 evolution and O_2 evolution reactions are realized at separate photocatalysts, these semiconductors could have bandgap energy values lower than 3 eV that would enable visible light utilization such as Pt- or RuO_2-loaded WO_3

Semiconductor	Co-catalyst	Bandgap (eV)	H_2 activity (μmol/h)	O_2 activity (μmol/h)	AQY (%)	Reference
$SrTiO_3$:Rh,Sb	IrO_2		4.4	1.9	0.1 at 420 nm	[71]
g-C_3N_4	Pt-CoO_x	2.8	~8.5	~3.5	0.3 at 405 nm	[72]
CDots-C_3N_4		2.74	46		16 at 420 nm	[70]
$Bi_{1-x}In_xV_{1-x}Mo_xO_4$	RuO_2	2.5	17		3.2 at 420 nm	[73]
$BiYWO_6$	RuO_2	2.7	4.1	1.8	0.17 at 420 nm	[74]
$LaMg_{1/3}Ta_{2/3}O_2N$	$RhCrO_x$		22	11	0.18 at 440 nm	[75]
$(Zn_{0.18}Ga_{0.82})(N_{0.82}O_{0.18})$	$Rh_{2-y}Cr_yO_3$	2.64	927	460	5.9 at 420 nm	[76]
GaN:Mg/InGaN:Mg	Rh/Cr_2O_3	2.22	38	21	12.3 at 400 nm	[69]

Table 2.
H_2 and O_2 evolution activity of one-step water splitting catalysts under visible light irradiation.

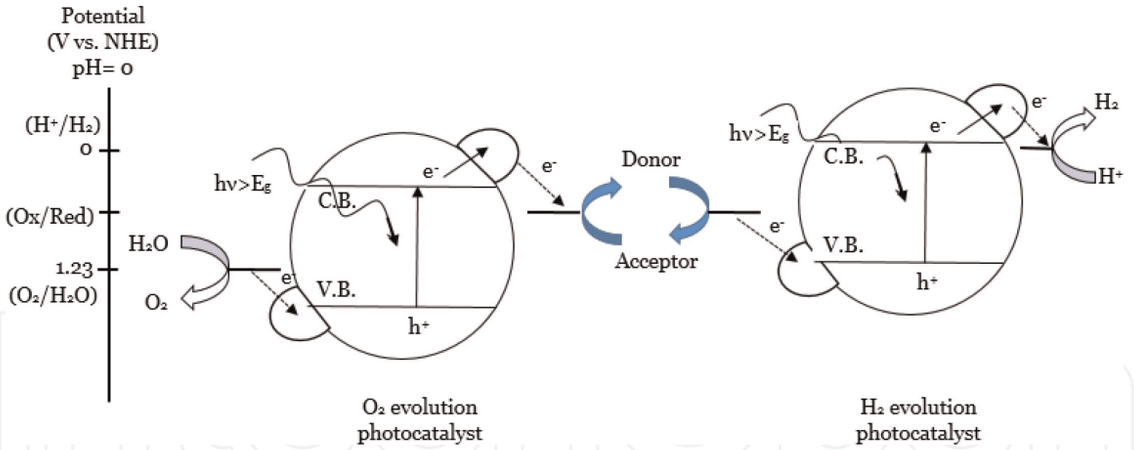

Figure 2.
Schematic diagram for photocatalytic water splitting using a two-step photoexcitation system.

H_2 photocatalyst	O_2 photocatalyst	Mediator	H_2 activity (μmol/h)	O_2 activity (μmol/h)	AQY (%)	Reference
Pt/$SrTiO_3$:Rh	$BiVO_4$	Fe^{3+}/Fe^{2+}	15	7.2	0.4 at 420 nm	[77]
Pt/$SrTiO_3$:Cr/Ta	PtO_x/WO_3	IO_3^-/I^-	~16	~8	1 at 420 nm	[78]
Pt/TaON	PtO_x/WO_3	IO_3^-/I^-	~16.5	~8	0.5 at 420 nm	[79]
Pt/ZrO_2/TaON	PtO_x/WO_3	IO_3^-/I^-	52	27	6.3 at 420 nm	[80]
Ru/$SrTiO_3$:Rh	$BiVO_4$	Fe^{3+}/Fe^{2+}	88	44	4.2 at 420 nm	[81]
Pt/$MgTa_2O_{6-x}N_y$/ TaON	PtO_x/WO_3	IO_3^-/I^-	108	55	6.8 at 420 nm	[82]

Table 3.
Z-scheme-type photocatalysts for water splitting without sacrificial agents.

($E_g \sim 2.8$ eV) or oxynitrides such as TaON ($E_g \sim 2.4$ eV) or Rh-doped $SrTiO_3$ ($E_g \sim 2.4$ eV). Examples of these materials and systems can be seen in **Table 3**. The detailed reviews on two-step photocatalytic water splitting can be found elsewhere [83].

3. Drawbacks on photocatalytic activity

There are numerous and challenging processes that need to be realized for photocatalytic evolution of H_2 and O_2 (**Table 4**) via a thermodynamically unfavorable reaction (Eq. (3)):

$$H_2O \rightarrow H_2 + 1/2\ O_2\ \Delta G^0 = 237\ \text{kJ/mol} \quad (3)$$

These processes include (i) excitation of the semiconductor photocatalyst with photon having higher energies than the bandgap energy of the material, (ii) transfer of the photo-generated electrons and holes to the reaction sites on the surface, (iii) utilization of these charge carriers in the oxidation/reduction reactions, and (iv) desorption of the products from the surface of the photocatalyst to the liquid/gas medium.

As the timescale of these processes varies, recombination of the electrons and holes in the bulk or on the surface happens more frequently than the rate of the

Process		Timescale
Light absorption and electron and hole generation	$Semiconductor \xrightarrow{h\nu} e^- + h^+$	fs
Photo-generated electron and hole transfer to the surface and trapping	$h^+_{VB} \rightarrow h^+_{trap}$ $e^-_{CB} \rightarrow e^-_{trap}$	200 fs 50 ps
Recombination of charge carriers	$e^-_{tr} + h^+_{tr} \rightarrow recombination$	>20 ns
Interfacial charge transfer	$e^-_{CB} + O_2 \rightarrow O_2^{\bullet -}$	10–100 μs
Observed O_2 evolution*	$2H_2O + 4h^+ \rightarrow O_2 + 4H^+$	37 s*
Photosynthesis of H_2O oxidation	$2H_2O + 4D^+TA \rightarrow O_2 + 4H^+ + DTA$	1.59 ms [84]

**Based on 16,000 μmol O_2/g/h O_2 evolution rate on $Rh_{0.5}Cr_{1.5}O_3$-doped Ga_2O_3:Zn upon illumination at 254 nm [41], assuming 10 m^2/g surface area and 10^{15} sites/cm^2 site density.*

Table 4.
The processes occurring in photocatalytic water splitting on TiO_2 and their timescales [27] and the references therein.

chemical oxidation/reduction reactions. Recombination is therefore considered to be one of the main reasons limiting the photocatalytic activity. Together with the recombination events, realization of back-oxidation reactions (Eq. (4)) on noble metals and the rate-limiting mass transfer events are the major drawbacks in an efficient photocatalytic process:

$$H_2 + 1/2O_2 \rightarrow H_2O\ \Delta G^0 = -237\ \text{kJ/mol} \tag{4}$$

Natural photosynthesis yields a much higher rate of O_2 evolution (see **Table 4**) when compared to artificial water splitting due to improved charge carrier and mass transfer events. From this comparison, it is clear that the photocatalytic systems still need to be perfected to compete with the nature's intricate design.

3.1 Charge recombination

Due to the presence of the multiple processes, the overall photocatalytic reactions are extremely complicated. In order to obtain an efficient photocatalytic performance, the photo-generated charges must be transferred to the surface reaction sites as rapidly as possible while preventing recombination or trapping of these charge carriers. It is reported by Leytner and Hupp that 60% of the trapped electron–hole pairs recombine with a timescale of about 25 ns while releasing heat of 154 kJ/mol [85]. As the defects such as vacancies and dislocations are considered as recombination sites, higher crystallinity of the photocatalysts is often aimed to decrease the recombination rates. From diffusion point of view, the shorter distances for the charge carriers to the surface reaction centers are also aimed to prevent the recombination. Shorter pathways are achieved via smaller crystal/particle sizes of the photocatalysts. More than two times of increase in the H_2 and O_2 evolution rates on Al-doped $SrTiO_3$ photocatalyst (reaching an apparent quantum yield of 56% [45]) as the particle size drops from few micrometers to 200 nm is a direct evidence of the effect of the particle size. Another method for reducing the charge recombination is to make use of phase junctions. One example is the α-β-phase junction of Ga_2O_3, which results in enhanced interfacial charge transfer, charge separation, and therefore enhanced water splitting activity [86]. Loading the photocatalysts with co-catalysts such as noble metals or transition metal oxides to accelerate the reduction/oxidation reactions is a commonly employed method.

These co-catalysts are known to enhance the charge migration from the semiconductor depending on the alignment of the potentials of the semiconductor and the co-catalyst. As these co-catalysts accelerate the desired H_2 evolution and O_2 evolution reactions, they can also increase the rates of undesired secondary reactions such as hydrogen oxidation or oxygen reduction to water reactions.

3.2 Back-oxidation reactions

Introduction of one-step photocatalysts for overall water splitting combined the H_2 evolution and O_2 evolution sites on the same catalyst surface. This design of a photocatalytic system that realizes both charge trapping and reduction/oxidation reactions on the same surface not only accelerated the charge recombination but also allowed secondary reactions on these reduction/oxidation centers. When fast removal of the products, i.e., H_2 and O_2, is not provided and there are no barriers that prevent interaction of these products with highly active sites, the reaction of H_2 and O_2 on the photocatalyst surface to produce H_2O ($2H_2 + O_2 \rightarrow H_2O$) is highly probable. And back-oxidation of the produced H_2 is considered to be one of the main reasons for observed low photocatalytic water splitting activity values.

As early as 1985, Sato and coworkers realized the importance of back-oxidation of H_2 with O_2 to produce H_2O. They have realized that the metal-loaded photocatalysts, mainly Pt- or Pd-loaded TiO_2, can oxidize H_2 with O_2 easily under the same photocatalytic water oxidation conditions. They have reported first-order reaction rate constants in the range of 0.23–0.51 h^{-1} for Pt, 0.32–1.8 h^{-1} for Pd, and 0.2–0.3 h^{-1} for Rh, suggesting the least active metal for back-oxidation reaction to be Rh [10]. Later in 2000, Anpo and coworkers investigated back-oxidation reaction on Pt/TiO_2 systems under dark conditions and observed increased back-oxidation rate with increasing Pt loading (up to 0.1 wt.% [87]). While Pt is active for H_2 evolution (Eq. (1)), it is also notoriously active for dark H_2–O_2 recombination reaction (Eq. (4)) even at room temperature [88]. In order to prevent H_2–O_2 recombination reaction, the Pt surface is modified with F ions for Pt/TiO_2 catalyst, and the reaction rate decreased from 2 to 0.3 h^{-1} upon F^- modification [89]. The inhibition mechanism is suggested to be due to the occupation of the H_2 surface adsorption sites on Pt by F atoms.

Another modification to the noble metal surfaces is reported by Lercher et al., in which CO is chemisorbed on the Rh co-catalyst for GaN:ZnO semiconductor. Chemisorbed molecular layer of CO suppressed the back-oxidation reaction by selective metal poisoning of the back-oxidation sites by CO. While H_2 evolution rates of 28 μmol/h are achieved (75 mg photocatalyst, 300 W Xe lamp [90]), significant CO oxidation to CO_2 is also observed.

The back-oxidation reaction-inhibiting effects of the nanolayer coating on noble metals are shown on Rh/Cr_2O_3-loaded GaN:ZnO photocatalysts. Rh/Cr_2O_3 core-shell structure [91] is formed by photodeposition of Rh and reduction of CrO_4^{2-} by electrons coming from Rh upon radiation, resulting in few nanometer thickness of Cr_2O_3 layer (2–3 nm, see **Figure 3**). Hydrated Cr_2O_3 nanolayer is reported to selectively permeate protons for H_2 evolution reaction [92], whereas it hinders O_2 permeation from the layer inhibiting O_2 reduction reaction (Eq. (5)) on Rh sites [93]. The same effect is also valid for Cr_2O_3-coated Pt catalyst (GaN:ZnO). Back-oxidation rates on Pt-loaded GaN:ZnO photocatalyst decreased significantly from $\sim 105 \times 10^{-12}$ molecules/s to $\sim 8 \times 10^{-12}$ molecules/s, while photocatalytic H_2 evolution rate increased from $\sim 5 \times 10^{-12}$ molecules/s to $\sim 30 \times 10^{-12}$ molecules/s upon Cr_2O_3 coating [93]. Apart from the oxygen-blocking role of the Cr_2O_3 nanolayer, much lower back-oxidation rate of Rh-loaded GaN:ZnO when compared to Pt-loaded GaN:ZnO (11×10^{-12} molecules/s vs. 105×10^{-12} molecules/s)

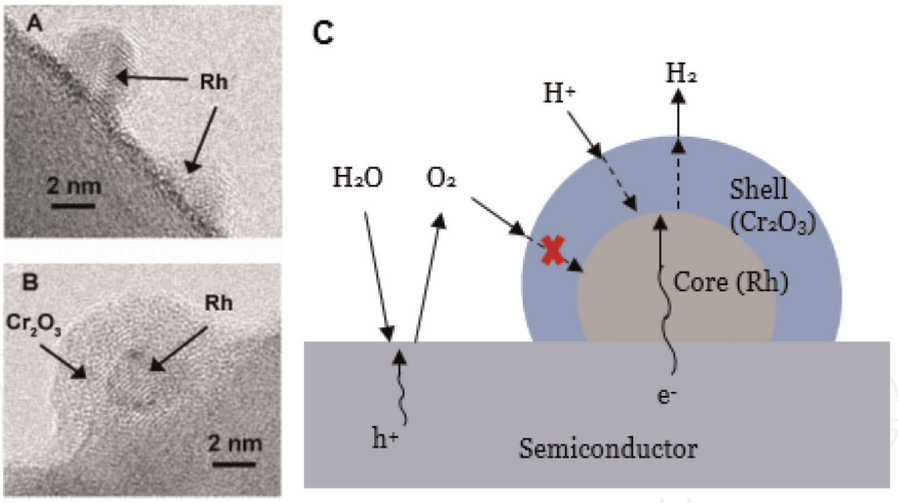

Figure 3.
HR-TEM images of GaN:ZnO photodeposited with (A) Rh and (B) Rh/Cr_2O_3. Reprinted with permission from [55]. Copyright 2007 American Chemical Society. (C) Schematic representation of O_2 and H_2 evolution reactions with inhibited O_2 permeation and O_2 reduction reaction on core-shell-type co-catalysts.

explains the significant photocatalytic H_2 evolution activity on Rh/Cr_2O_3-loaded GaN:ZnO (130×10^{-12} molecules/s). Lower back-oxidation rate of Rh-loaded GaN:ZnO could be related to the low-oxygen reduction reaction (Eq. 5) activity of Rh when compared to Pt [94]:

$$O_2 + 4H^+ + 4e^- \rightarrow 2H_2O \tag{5}$$

Similar selective permeability concept is considered to be the case for Ni/NiO core-shell structures deposited on various photocatalysts such as $SrTiO_3$ or $NaTaO_3$ [34, 57]. In these systems, in addition to the back-oxidation reaction impeding effect of NiO layer on Ni [58], low-oxygen reduction activity of NiO_x catalysts when compared to Pt can also be considered to be effective for improved water splitting activity.

Coatings of the whole photocatalyst instead of the co-catalyst by oxyhydroxides of Ti, Nb, and Ta are reported on Rh-loaded $SrTiO_3$:Sc photocatalyst. Surface nanolayer not only suppressed back-oxidation reactions but also prevented the access of sacrificial agents such as ethanol to the photocatalyst surface, resulting in nearly stoichiometric H_2/O_2 ratios [95]. Surface nanolayer coatings on the whole photocatalysts have proven to also prevent photodecomposition (N_2 evolution) of oxynitride photocatalysts while increasing the overall water splitting activity [64, 68].

Prevention of the secondary reactions such as H_2 oxidation or O_2 reduction reaction to H_2O is found to be essential for improving the overall water splitting activity and the apparent quantum yield values (reaching apparent quantum yield value of 69% under irradiation at 365 nm [40]). In addition to the reduced back-oxidation rates, complementary measures such as decreasing the charge recombination rates and enhancing the product transfer rates away from the surface (increasing the mass transfer rates) are necessary for increased photocatalytic water splitting activity.

3.3 Mass transfer limitations

Mass transfer limitations especially in the slurry photocatalytic systems can be the most overlooked problem in the photocatalytic field. To complete the

photocatalytic reaction cycle, adsorption of the reactants, reduction/oxidation of the reactants, desorption of the products, and transfer of the products from the photocatalyst surface to the gas phase need to be realized. When the rates of the mass transfer of the products from the surface are slower than the reduction/oxidation rates, produced H_2 and O_2 would stay longer on the surface, resulting in promotion of back-oxidation reactions. Moreover, when the mass transfer rates are slower than the reaction kinetics, the apparent H_2 and O_2 evolution rates in the gas phase will be limited by the mass transfer rates.

Experimental evidence for mass transfer limitations in agitated systems is presented in a previous publication [96]. In a batch slurry reactor, where the catalyst particles are suspended via agitation, observed H_2 evolution rates for UV-irradiated Pt/TiO_2 photocatalyst showed improvement with increasing stirring rates up to 900 rpm (**Figure 4a**). This improvement is a direct indication of mass transfer limitations on the solid–liquid and gas–liquid interfaces as the turbulence in the liquid and therefore boundary layers are affected by increasing stirring rates. In another experiment, the effect of liquid volume is investigated by varying catalyst

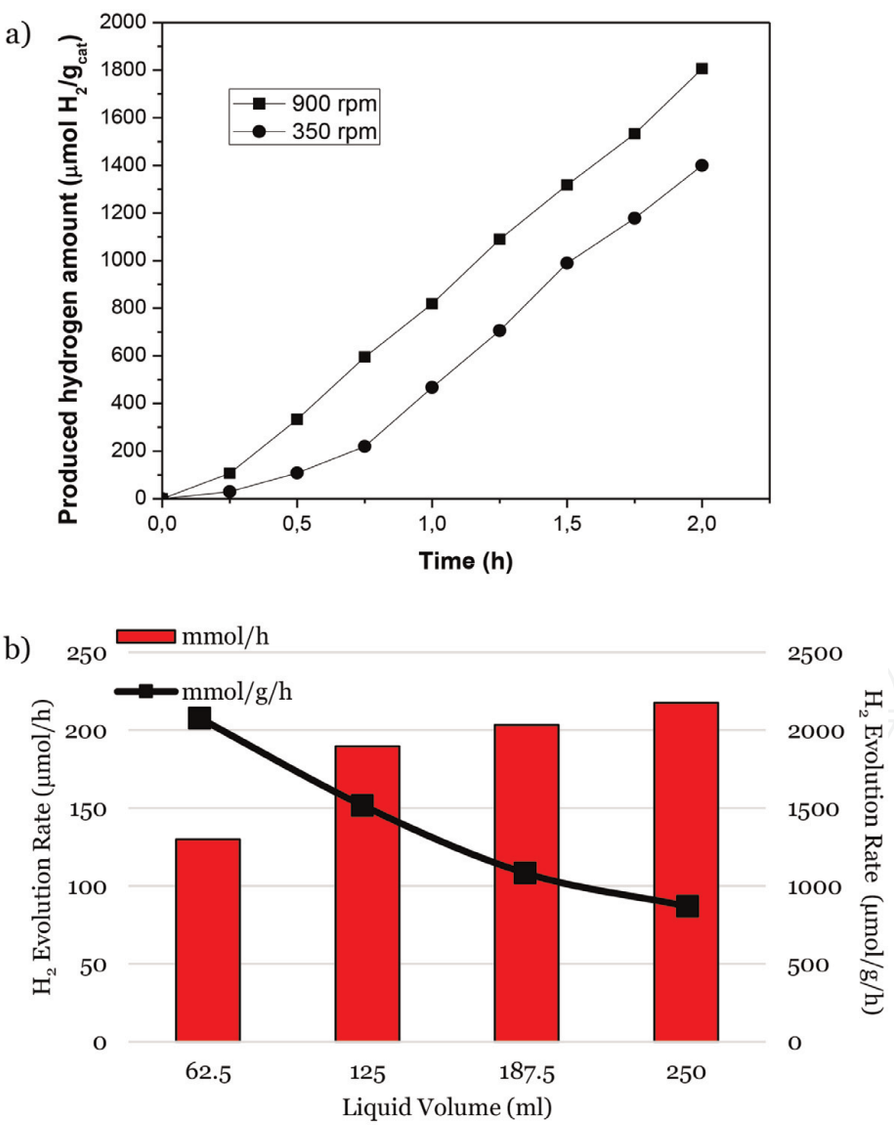

Figure 4.
(a) Effect of stirring rate on photocatalytic hydrogen evolution with methanol as sacrificial agent, with 0.5 wt% Pt/TiO_2, 250 ml deionized water, 2 ml methanol, (■) 900 rpm and (●) 350 rpm. (b) Observed hydrogen evolution rates in the gas phase with changing liquid volume, CH_3OH/H_2O:1/125 (v/v) and $C_{catalyst}$: 1 g/L for each case. Adapted from [96].

weight and liquid volumes (keeping the catalyst concentration constant). H_2 evolution rates on an hour basis (μmol H_2/h) are found the same regardless of the liquid volume (or catalyst weight) above 62.5 ml (**Figure 4b**) as the H_2 evolution rate per gram and hour basis decreased as liquid volume increased. Similar H_2 evolution rates regardless of the catalyst weight indicate significant mass transfer limitations in the liquid–gas interface.

Mass transfer limitations for different photocatalytic reaction systems are analyzed by different groups. For immobilized photocatalyst systems, the importance of internal mass transfer resistance is emphasized [97]. In another investigation, severe mass transfer limitations are observed in the product separator (liquid–gas interface) for a fluidized bed/separator system, in which modification of the liquid–gas surface area enhanced the H_2 evolution rates by 350% [98].

To prevent mass transfer limitations in the photocatalytic tests and to report actual kinetic rates; stirring rates, liquid levels, and mass transfer areas should be designed carefully. To design these parameters, approximate mass transfer rates should be known. Here, we present a sample calculation for H_2 mass transfer rate in a slurry reactor containing 0.5 g TiO_2 photocatalyst having a surface area of 40 m^2/g inside an agitated glass reactor having 200 ml liquid volume and a tank diameter of 7 cm.

Mass transfer resistances in a gas–liquid–solid multiphase photocatalytic systems involve the internal mass transfer, mass transfer from the solid catalyst particles to liquid (Eq. 6), transfer from the liquid bulk to the liquid interface (Eq. 7), and transfer from the liquid–gas interface to the gas phase (Eq. 8). Photocatalysts such as perovskites and TiO_2 are known to be nonporous (unless mesoporous versions are prepared on purpose [99, 100]) and have surface area values between 5 and 50 m^2/g. For nonporous photocatalysts, the internal mass transfer limitations can be discarded (Eq. 9). Hence, the H_2 mass transfer rate equation will have a form containing the mass transfer resistances from the solid–liquid and liquid–gas interfaces as seen in Eq. 8:

$$r_{H2,S} = k_s a_S (C_S - C_L) \tag{6}$$

$$r_{H2,L} = k_L a_L (C_L - C_{L,i}) \tag{7}$$

$$r_{H2,G} = k_G a_G (C_{G,i} - C_G) \tag{8}$$

$$r_{H2} = \frac{C_{H2,s} - HC_{H2,g}}{\left(\frac{1}{k_s a_S} + \frac{1}{k_L a_L} + \frac{H}{k_G a_G}\right)} \tag{9}$$

The mass transfer limitations coming from the solid–liquid and liquid–gas interfaces may play important role depending on the photocatalytic reactor type. The most often used photocatalytic reactor systems such as slurry reactors have solid–liquid and liquid–gas phase interfaces that suspend its catalysts by agitation using an impeller or a magnetic stirrer. The convection mass transfer coefficient for solid–liquid interface of such a system could be estimated using Eq. 10 suggested by Armenante and Kirwan for agitated tanks using Kolmogorov's theory for Reynold's number calculation to consider the effect of solid particle size [101]:

$$Sh = \frac{k_s d_p}{D_{H2-H2O}} = 2 + 0.52\,\mathrm{Re}^{0.52} Sc^{1/3} \tag{10}$$

where k_s is the convection mass transfer coefficient from solid to liquid in (m/s), d_p is the particle diameter in (m), D_{H2-H2O} is the diffusion coefficient of H_2 in liquid water (m^2/s), and Sc is the Schmidt number. A rough estimation for k_s for such system can be found in **Table 5**.

The creation of air/inert bubbles in the continuous phase (water) due to agitation could be considered as the transfer mechanism of produced H_2 from the liquid phase to the gas phase. In such systems, comparing the mass transfer resistance from liquid to interface and interface to gas, it can be assumed that nearly all of the mass transfer resistance comes from the liquid side of the interface [102], leaving Eq. 9 as Eq. 11:

$$r_{H2} = \frac{C_{H2,s} - C_{H2,Li}}{\left(\frac{1}{k_s a_S} + \frac{1}{k_L a_L}\right)} \tag{11}$$

The liquid side mass transfer coefficient for such a system could then be calculated using Calderbank and Moo-Young correlation for rising small bubbles of gas in continuous liquid phase (Eq. 12) [103]:

$$Sh = \frac{k_L d_b}{D_{H2-H2O}} = 2 + 0.31 Ra^{1/3} \; where \; Ra = \frac{d_b^3(\rho_L - \rho_G)g}{\mu_L D_{H2-H2O}} \tag{12}$$

The first term on Eq. 12 is the molecular diffusion term, whereas the second term is for the rise of the bubbles due to gravitational forces independent of the agitation. With estimations on the bubble size and gas holdup of such a system (given in **Table 6**), the mass transfer coefficient and $k_L a_L$ term are calculated to be 2.5×10^{-4} m/s and 2.2×10^{-6} m^3/s, rendering liquid–gas mass transfer resistance way more important than solid–liquid resistance.

The overall mass transfer coefficient and the mass transfer rate from solid to the gas phase can be calculated with the estimated $k_s a_S$ and $k_L a_L$ values. As the concentration of H_2 in the gas phase will be negligible ($C_G \sim 0$), the liquid phase interface can also be assumed to be equal to zero ($C_{H2,Li} \sim 0$) with negligible gas phase resistance. Therefore, from Eq. 11, the rate of H_2 mass transfer can be calculated by assuming H_2 concentration at the catalyst surface and the gas holdup ratio in the liquid. The rate of H_2 mass transfer values for 200 ml of water and 0.5 g of catalyst

Parameter	Unit	Value
Particle size, d_p	μm	1
Density of water, ρ_L	kg/m^3	997 at 25°C
Viscosity of water, μ_L	Pa s	890×10^{-6} at 25°C
Kinematic viscosity, ν	m^2/s	8.93×10^{-7}
Schmidt number $\left(Sc = \nu/D_{H2-H2O}\right)$		141
Energy density, $\varepsilon = \frac{Power}{mass\ of\ liquid}$	m^2/s^3	25 for 5 W stirrer, 200 g solution
Reynold's number $\left(\mathrm{Re} = \varepsilon^{1/3} d_p^{4/3}/\nu\right)$		0.033
Sherwood number, $Sh = \frac{k_s d_p}{D_{H2-H2O}} = 2 + 0.52\,\mathrm{Re}^{0.52} Sc^{1/3}$		2.46
Diffusion coefficient of H_2 in water	m^2/s	$6.30{*}10^{-9}$ at 25 °C
Convection mass transfer coefficient for solid, k_s	m/s	0.015
$k_s a_S$	m^3/s	0.31

Table 5.
Convection mass transfer coefficient calculation for solid–liquid transfer and parameters used in the calculation.

are calculated in the range of ~200–8000 μmol/h (see **Figure 5**) for a surface H_2 adsorption capacity range of 50–400 μmol/g (H_2 chemisorption on 0.1% Pt/TiO_2 is reported to be ~400 μmol/g at room temperature [104]) and gas holdup ratio between 0.001 and 0.005.

The H_2 concentration on the solid surface and the gas–liquid contact area are not easy to estimate. However, for the limited gas–liquid area, the photocatalytic reaction rates above the calculated mass transfer rate will be suppressed due to the limiting mass transfer rates. Therefore, special care must be given for the UV-irradiated photocatalytic systems, in which observed H_2 and O_2 evolution rates are found to be close to the calculated mass transfer rates here (see **Table 1**).

These studies show that for each type of photocatalytic system that contains limited gas–liquid contact area or immobilized photocatalyst, mass transfer limitations should not be underestimated, and not only the materials but also the systems should be improved for better photocatalytic efficiencies.

Parameter	Unit	Value
Bubble size, d_b	μm	700
Density of water, ρ_L	kg/m^3	997 at 25°C
Density of air, ρ_G	kg/m^3	1.18 at 25°C
Viscosity of water, μ_L	Pa s	890×10^{-6} at 25°C
Raleigh number $\left(Ra = \frac{d_b^3(\rho_L - \rho_G)g}{\mu_L D_{H2-H2O}}\right)$		5.97×10^5
Sherwood number, $Sh = \frac{k_L d_b}{D_{H2-H2O}} = 2 + 0.31Ra^{1/3}$		28.1
Diffusion coefficient of H_2 in water	m^2/s	6.3×10^{-9} at 25°C
Convection mass transfer coefficient for liquid, k_L	m/s	2.5×10^{-4}
Liquid–gas bubble contact area, $a_L = \frac{6V_G}{d_b} = \frac{6\phi}{d_b}V_L$ *where* $\phi = V_G/V_L$	m^2	0.008 (gas holdup, ϕ, assumed to be 0.005)
$k_L a_L$	m^3/s	2.2×10^{-6}

Table 6.
Convection mass transfer coefficient calculation for liquid–gas transfer and parameters used in the calculation.

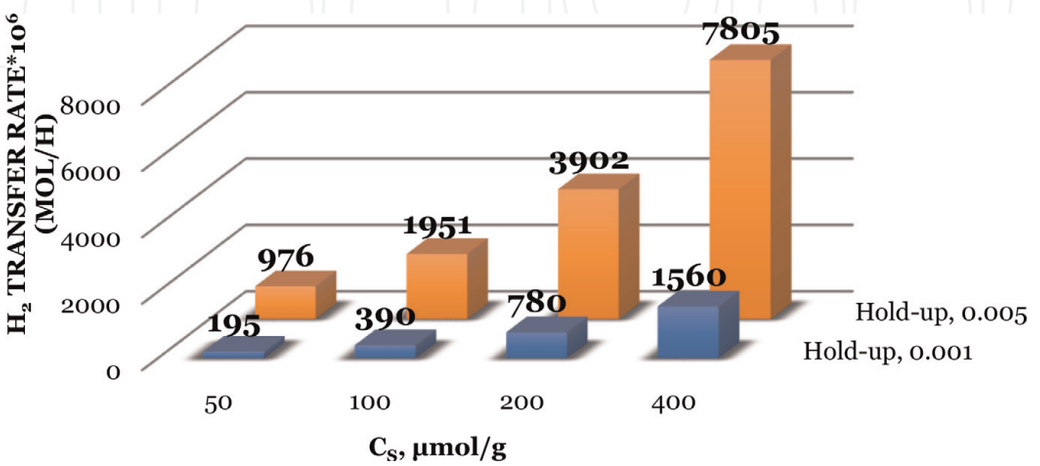

Figure 5.
Calculated H_2 mass transfer rate values (μmol H_2/h) for gas holdup values of 0.001 and 0.005 and H_2 adsorption capacity values in the range of 50–400 μmol/g. The liquid volume is taken as 200 ml and catalyst weight is taken as 0.5 g.

4. Future of photocatalytic H_2 evolution

The literature examples of photocatalytic water splitting activities show improvements in visible light utilization, charge separation, and prevention of back-oxidation reactions via fine tuning of photocatalyst materials that enabled more efficient water splitting systems. The efficiency of these systems working under sunlight is better defined with solar-to-hydrogen energy conversion efficiency (STH), i.e., hydrogen production rate times the Gibbs free energy for generating 1 mole of H_2 divided by the power of incident sunlight (Eq. 13):

$$STH = \frac{(mmol\ H_2/s) * 237 * 10^3\ J/mol}{P\left(\frac{mW}{cm^2}\right) * A(cm^2)} \times 100 \quad (13)$$

The estimated STH required for the particulate photocatalytic systems to be economically compatible with current H_2 production technologies is 10% [104]. However, the highest STH values obtained with current developed photocatalysts are in the order of 1–2% (1.8% at 400–475 nm using Rh/Cr_2O_3-loaded GaN:Mg/InGaN:Mg photocatalyst [69] and 2% at 420 nm using CDots-C_3N_4 [70]). The STH conversion efficiency depends both on the catalytic activity and the extent of the utilization of sunlight that depends on the bandgap of the semiconductor. With current photocatalysts having absorption edges around 500 nm, even 100% apparent quantum yields would not guarantee 10% STH values [106]. For a photocatalyst to show 10% STH values, it should have absorption edges at least at 600 nm with apparent quantum yields around 60%. Under the light of these calculations, it can be said that the present photocatalysts having adsorption edge values around 450 nm and quantum yields around 10% are far from being utilized in commercial systems. In order to achieve targeted STH values, the photocatalysts with lower bandgap energies such as (oxy)nitrides and (oxy)sulfides should be improved for H_2 evolution activities while ensuring their thermal stability and photostability.

Large-scale photocatalytic water splitting reactors are implemented with current low STH values as of 2015. The first example of large-scale photocatalytic water splitting utilized Pt-loaded C_3N_4 photocatalyst with sacrificial electron donor triethanolamine in a flat-panel-type photocatalytic reactor system in 2015 [107]. The solar-to-hydrogen conversion efficiency is reported to be 0.12%, for which the photocatalytic activity is monitored for 30 days. In such systems, where a sacrificial reagent such as triethanolamine or methanol is irreversibly oxidized at a more negative potential than water (thermodynamically more favorable) at the oxidation centers, the photo-generated charges can be more efficiently separated, thus increasing H_2 evolution rates. However, in those systems, hydrogen production is not solely due to the water splitting; as the carbon- and hydrogen-containing "sacrificial agents" are being oxidized at the oxidation centers, they produce hydrogen as well as aldehydes, carboxylic acid, and carbon dioxide [108].

Another large-scale photoreactor is reported by Domen et al., who used Al-doped and $RhCrO_x$-loaded $SrTiO_3$ photocatalyst sheets in their 1×1 m water splitting panel [45]. The achieved STH value under simulated sunlight is 0.6% at 331 K and limited to a maximum value of 1.4% due to the large bandgap energy of the photocatalyst (3.2 eV). Improved STH values (reaching 1.1%) are shown to be possible on a two-step excitation system in 2016 using photocatalyst sheets having smaller bandgap energy values such as Mo-doped $BiVO_4$ (2.4 eV) and La- and Rh-doped $SrTiO_3$ [5].

5. Conclusion

The developments in the photocatalytic water splitting reactions are explained here with the emphasis on the one-step photocatalysis systems. The early photocatalyst improvements with bandgap engineering, co-catalyst usage, and size reductions are shown to contribute to the increased visible light-driven H_2 evolution activity values. The main drawbacks in the present systems are discussed to be the charge recombination, back-oxidation reactions of the products into water, and mass transfer limitations especially in the three-phase systems. Using defect-free small crystals of photocatalysts and making use of phase junctions or metal co-catalysts are suggested to decrease charge recombination rates. Back-oxidation of H_2 into water or oxygen reduction reaction to water is expected in many noble metal-containing particulate photocatalyst systems. The prevention of these unwanted secondary reactions is shown to be possible to some extent by modification of the noble metal surfaces. Some examples of these modifications are anion coating, partial adsorption of a poison, or nanolayer coating of the co-catalyst or the whole photocatalyst. Selective permeation property of the nanolayer coatings such as Cr_2O_3 is reported to suppress the back-oxidation rates, resulting in enhanced H_2 and O_2 evolution rates. Possible mass transfer limitations, limiting the observed rates in three-phase systems, are predicted especially in the liquid–gas interfaces. The literature examples attracted attention for the liquid–gas interfaces in suspended systems and internal mass transfer limitations for the immobilized photocatalyst systems. It is concluded that, in addition to the required developments in activities with suppression of charge recombination, back-oxidation, and mass transfer limitations, future of the photocatalytic systems would necessitate active and stable photocatalysts with narrower bandgap energies (to be activated at >600 nm) for achieving targeted 10% solar-to-hydrogen energy conversion efficiency value.

Author details

Bahar Ipek* and Deniz Uner
Department of Chemical Engineering, Middle East Technical University, Ankara, Turkey

*Address all correspondence to: bipek@metu.edu.tr

References

[1] Centi G, Perathoner S. Opportunities and prospects in the chemical recycling of carbon dioxide to fuels. Catalysis Today. 2009;**148**:191-205

[2] Erisman JW, Sutton MA, Galloway J, Klimont Z, Winiwarter W. How a century of ammonia synthesis changed the world. Nature Geoscience. 2008;**1**: 636-639

[3] Aasberg-Petersen K, Dybkjær I, Ovesen CV, Schjødt NC, Sehested J, Thomsen SG. Natural gas to synthesis gas—Catalysts and catalytic processes. Journal of Natural Gas Science and Engineering. 2011;**3**:423-459

[4] Morton O. A new day dawning?: Silicon valley sunrise. Nature. 2006;**32**: 19-22

[5] Wang Q, Hisatomi T, Jia Q, Tokudome H, Zhong M, Wang C, et al. Scalable water splitting on particulate photocatalyst sheets with a solar-to-hydrogen energy conversion efficiency exceeding 1%. Nature Materials. 2016; **15**:611-615

[6] Jia J, Seitz LC, Benck JD, Huo Y, Chen Y, Ng JWD, et al. Solar water splitting by photovoltaic-electrolysis with a solar-to-hydrogen efficiency over 30%. Nature Communications. 2016;**7**:1-6

[7] Fujishima A, Honda K. Electrochemical photolysis of water at a semiconductor electrode. Nature. 1972; **238**:37-38

[8] Sato S, White JM. Photodecomposition of water over Pt/TiO_2 catalysts. Chemical Physics Letters. 1980;**72**:83-86

[9] Wagner FT, Somorjai GA. Photocatalytic hydrogen production from water on Pt-free $SrTiO_3$ in alkali hydroxide solutions. Nature. 1980;**285**: 559-560

[10] Yamaguti K, Sato S. Photolysis of water over metallized powdered titanium dioxide. Journal of the Chemical Society, Faraday Transactions 1: Physical Chemistry in Condensed Phases. 1985;**81**:1237-1246

[11] Kudo A, Domen K, Ken-ichi M, Onishi T. Photocatalytic activities of TiO_2 loaded with NiO. Chemical Physics Letters. 1987;**133**:517-519

[12] Sayama K, Arakawa H. Effect of carbonate salt addition on the photocatalytic decomposition of liquid water over Pt-TiO_2 catalyst. Journal of the Chemical Society, Faraday Transactions. 1997;**93**:1647-1654

[13] Tabata S, Nishida H, Masaki Y, Tabata K. Stoichiometric photocatalytic decomposition of pure water in Pt/TiO_2 aqueous suspension system. Catalysis Letters. 1995;**34**:245-249

[14] Moon SC, Mametsuka H, Suzuki E, Anpo M. Stoichiometric decomposition of pure water over Pt-loaded Ti/B binary oxide under UV-radiation. Chemistry Letters. 1998;**27**:117-118

[15] Sayama K, Arakawa H. Effect of Na_2CO_3 addition on photocatalytic decomposition of liquid water over various semiconductor catalysts. Journal of Photochemistry and Photobiology A: Chemistry. 1994;**77**:243-247

[16] Bard AJ. Photoelectrochemistry. Science (80-). 1980;**207**:139-144

[17] Anpo M, Yamashita H, Ichihashi Y, Ehara S. Photocatalytic reduction of CO_2 with H_2O on various titanium oxide catalysts. Journal of Elcetroanalytical Chemistry. 1995;**396**:21-26

[18] Saladin F, Forss L, Kamber I. Photosynthesis of CH_4 at a TiO_2 surface from gaseous H_2O and CO_2. Journal of

the Chemical Society, Chemical Communications. 1995:533-534

[19] Yamashita H, Nishiguchi H, Kamada N, Anpo M, Teraoka Y, Hatano H, et al. Photocatalytic reduction of CO_2 with H_2O on TiO_2 and Cu/TiO_2 catalysts. Research on Chemical Intermediates. 1994;**20**:815-823

[20] Anpo M, Aikawa N, Kubokawa Y. Photocatalytic hydrogenation of alkynes and alkenes with water over TiO_2. Pt-loading effect on the primary processes. The Journal of Physical Chemistry. 1984;**88**:3998-4000

[21] Anpo M, Nakaya H, Kodama S, Kubokawa Y, Domen K, Onishi T. Photocatalysis over binary metal oxides. Enhancement of the photocatalytic activity of titanium dioxide in titanium-silicon oxides. The Journal of Physical Chemistry. 1986;**90**:1633-1636

[22] Choi W, Termin A, Hoffmann MR. The role of metal ion dopants in quantum-sized TiO_2: Correlation between photoreactivity and charge carrier recombination dynamics. The Journal of Physical Chemistry. 1994;**98**: 13669-13679

[23] Yamashita H, Ichihashi Y, Harada M, Stewart G, Fox MA, Anpo M. Photocatalytic degradation of 1-octanol on anchored titanium oxide and on TiO_2 powder catalysts. Journal of Catalysis. 1996;**158**:97-101

[24] Trillas M, Pujol M, Domènech X. Phenol photodegradation over titanium dioxide. Journal of Chemical Technology and Biotechnology. 1992;**55**: 85-90

[25] Hidaka H, Zhao J. Photodegradation of surfactants catalyzed by a TiO_2 semiconductor. Colloids and Surfaces. 1992;**67**:165-182

[26] Kitano M, Matsuoka M, Ueshima M, Anpo M. Recent developments in titanium oxide-based photocatalysts. Applied Catalysis A: General. 2007;**325**: 1-14

[27] Schneider J, Matsuoka M, Takeuchi M, Zhang J, Horiuchi Y, Anpo M, et al. Understanding TiO_2 photocatalysis: Mechanisms and materials. Chemical Reviews. 2014;**114**:9919-9986

[28] Gaya UI, Abdullah AH. Heterogeneous photocatalytic degradation of organic contaminants over titanium dioxide: A review of fundamentals, progress and problems. Journal of Photochemistry and Photobiology C: Photochemistry Reviews. 2008;**9**:1-12

[29] Asahi R, Morikawa T, Ohwaki T, Aoki K, Taga Y. Visible-light photocatalysis in nitrogen-doped titanium oxides. Science (80-). 2001; **293**:269-271

[30] Parayil SK, Kibombo HS, Wu CM, Peng R, Baltrusaitis J, Koodali RT. Enhanced photocatalytic water splitting activity of carbon-modified TiO_2 composite materials synthesized by a green synthetic approach. International Journal of Hydrogen Energy. 2012;**37**: 8257-8267

[31] Xing M, Qi D, Zhang J, Chen F, Tian B, Bagwas S, et al. Super-hydrophobic fluorination mesoporous MCF/TiO_2 composite as a high-performance photocatalyst. Journal of Catalysis. 2012; **294**:37-46

[32] Periyat P, Pillai SC, Mccormack DE, Colreavy J, Hinder SJ. Improved high-temperature stability and sun-light-driven photocatalytic activity of sulfur-doped anatase TiO_2. Journal of Physical Chemistry C. 2008;**112**:7644-7652

[33] Kitano M, Funatsu K, Matsuoka M, Ueshima M, Anpo M. Preparation of nitrogen-substituted TiO_2 thin film photocatalysts by the radio frequency magnetron sputtering deposition

method and their photocatalytic reactivity under visible light irradiation. The Journal of Physical Chemistry B. 2006;**110**:25266-25272

[34] Kato H, Asakura K, Kudo A. Highly efficient water splitting into H_2 and O_2 over lanthanum-doped $NaTaO_3$ photocatalysts with high crystallinity and surface nanostructure. Journal of the American Chemical Society. 2003; **125**:3082-3089

[35] Ham Y, Hisatomi T, Goto Y, Moriya Y, Sakata Y, Yamakata A, et al. Flux-mediated doping of $SrTiO_3$ photocatalysts for efficient overall water splitting. Journal of Materials Chemistry A. 2016;**4**:3027-3033

[36] Ikarashi K, Sato J, Kobayashi H, Saito N, Nishiyama H, Inoue Y. Photocatalysis for water decomposition by RuO_2-dispersed $ZnGa_2O_4$ with d10 configuration. The Journal of Physical Chemistry B. 2002;**106**:9048-9053

[37] Sato J, Saito N, Nishiyama H, Inoue Y. New photocatalyst group for water decomposition of RuO_2-loaded p-block metal (In, Sn, and Sb) oxides with d10 configuration. The Journal of Physical Chemistry. B. 2001;**105**:6061-6063

[38] Inoue Y. Photocatalytic water splitting by RuO_2-loaded metal oxides and nitrides with d0- and d10-related electronic configurations. Energy & Environmental Science. 2009;**2**:364-386

[39] Kudo A, Miseki Y. Heterogeneous photocatalyst materials for water splitting. Chemical Society Reviews. 2009;**38**:253-278

[40] Chiang TH, Lyu H, Hisatomi T, Goto Y, Takata T, Katayama M, et al. Efficient photocatalytic water splitting using Al-doped $SrTiO_3$ coloaded with molybdenum oxide and rhodium-chromium oxide. ACS Catalysis. 2018;**8**: 2782-2788

[41] Sakata Y, Hayashi T, Yasunaga R, Yanaga N, Imamura H. Remarkably high apparent quantum yield of the overall photocatalytic H_2O splitting achieved by utilizing Zn ion added Ga_2O_3 prepared using dilute $CaCl_2$ solution. Chemical Communications. Royal Society of Chemistry. 2015;**51**: 12935-12938

[42] Chen X, Shen S, Guo L, Mao SS. Semiconductor-based photocatalytic hydrogen generation. Chemical Reviews. 2010;**110**:6503-6570

[43] Chen S, Takata T, Domen K. Particulate photocatalysts for overall water splitting. Nature Reviews Materials. 2017;**2**:1-17

[44] Kim J, Hwang DW, Kim HG, Bae SW, Lee JS, Li W, et al. Highly efficient overall water splitting through optimization of preparation and operation conditions of layered perovskite photocatalysts. Topics in Catalysis. 2005;**35**:295-303

[45] Goto Y, Hisatomi T, Wang Q, Higashi T, Ishikiriyama K, Maeda T, et al. A particulate photocatalyst water-splitting panel for large-scale solar hydrogen generation. Joule. 2018;**2**:509-520

[46] Kato H, Kudo A. Water splitting into H_2 and O_2 on alkali tantalate photocatalysts $ATaO_3$ (A = Li, Na, and K). The Journal of Physical Chemistry B. 2001;**105**:4285-4292

[47] Sakata Y, Matsuda Y, Yanagida T, Hirata K, Imamura H, Teramura K. Effect of metal ion addition in a Ni supported Ga_2O_3 photocatalyst on the photocatalytic overall splitting of H2O. Catalysis Letters. 2008;**125**:22-26

[48] Inoue Y, Niiyama T, Asai Y, Sato K. Stable photocatalytic activity of $BaTi_4O_9$ combined with ruthenium oxide for decomposition of water. Journal of

Chemical Society, Chemical Communications. 1992:579-580

[49] Iwase A, Kato H, Kudo A. Nanosized Au particles as an efficient cocatalyst for photocatalytic overall water splitting. Catalysis Letters. 2006; **108**:7-10

[50] Murdoch M, Waterhouse GIN, Nadeem MA, Metson JB, Keane MA, Howe RF, et al. The effect of gold loading and particle size on photocatalytic hydrogen production from ethanol over Au/TiO_2 nanoparticles. Nature Chemistry. 2011; **3**:489-492

[51] Li R, Han H, Zhang F, Wang D, Li C. Highly efficient photocatalysts constructed by rational assembly of dual-cocatalysts separately on different facets of $BiVO_4$. Energy & Environmental Science. 2014;**7**:1369-1376

[52] Liu L, Ji Z, Zou W, Gu X, Deng Y, Gao F, et al. In situ loading transition metal oxide clusters on TiO_2 nanosheets as co-catalysts for exceptional high photoactivity. ACS Catalysis. 2013;**3**: 2052-2061

[53] Maeda K, Wang X, Nishihara Y, Lu D, Antonietti M, Domen K. Photocatalytic activities of graphitic carbon nitride powder for water reduction and oxidation under visible light. Journal of Physical Chemistry C. 2009;**113**:4940-4947

[54] Youngblood WJ, Lee S-HA, Kobayashi Y, Hernandez-Pagan EA, Hoertz PG, Moore TA, et al. Photoassisted overall water splitting in a visible light-absorbing dye-sensitized photoelectrochemical cell. Journal of the American Chemical Society. 2009;**131**: 926-927

[55] Maeda K, Domen K. New non-oxide photocatalysts designed for overall water splitting under visible light. Journal of Physical Chemistry C. 2007; **111**:7851-7861

[56] Kamata K, Maeda K, Lu D, Kako Y, Domen K. Synthesis and photocatalytic activity of gallium-zinc-indium mixed oxynitride for hydrogen and oxygen evolution under visible light. Chemical Physics Letters. 2009;**470**:90-94

[57] Domen K, Naito S, Soma M, Onishi T, Tamaru K. Photocatalytic decomposition of water vapour on an $NiO–SrTiO_3$ catalyst. Journal of the Chemical Society, Chemical Communications. 1980:543-544

[58] Domen K, Kudo A, Onishi T, Kosugi N, Kuroda H. Photocatalytic decomposition of water into H_2 and O_2 over $NiO\text{-}SrTiO_3$ powder. 1. Structure of the catalysts. Journal of Physical Chemistry A. 1986;**90**:292-295

[59] Kim HG, Hwang DW, Kim J, Kim YG, Lee JS. Highly donor-doped (1 1 0) layered perovskite materials as novel photocatalysts for overall water splitting. Chemical Communications. 1999;**2**:1077-1078

[60] Sayama K, Arakawa H, Domen K. Photocatalytic water splitting on nickel intercalated $A_4Ta_xNb_{6-x}O_{17}$ (A = K, Rb). Catalysis Today. 1996;**28**:175-182

[61] Thaminimulla CTK, Takata T, Hara M, Kondo JN, Domen K. Effect of chromium addition for photocatalytic overall water splitting on Ni-$K_2La_2Ti_3O_{10}$. Journal of Catalysis. 2000; **196**:362-365

[62] Maeda K, Teramura K, Saito N, Inoue Y, Domen K. Improvement of photocatalytic activity of $(Ga_{1-x}Zn_x)$ $(N_{1-x}O_x)$ solid solution for overall water splitting by co-loading Cr and another transition metal. Journal of Catalysis. 2006;**243**:303-308

[63] Maeda K, Teramura K, Lu D, Saito N, Inoue Y, Domen K. Noble-

metal/Cr_2O_3 core/shell nanoparticles as a cocatalyst for photocatalytic overall water splitting. Angewandte Chemie International Edition. 2006;**45**:7806-7809

[64] Pan C, Takata T, Nakabayashi M, Matsumoto T, Shibata N, Ikuhara Y, et al. A complex perovskite-type oxynitride: The first photocatalyst for water splitting operable at up to 600 nm. Angewandte Chemie International Edition. 2015;**54**:2955-2959

[65] Ohno T, Bai L, Hisatomi T, Maeda K, Domen K. Photocatalytic water splitting using modified GaN:ZnO solid solution under visible light: Long-time operation and regeneration of activity. Journal of the American Chemical Society. 2012;**134**:8254-8259

[66] Maeda K, Teramura K, Takata T, Hara M, Saito N, Toda K, et al. Overall water splitting on $(Ga_{1-x}Zn_x)(N_{1-x}O_x)$ solid solution photocatalyst: Relationship between physical properties and photocatalytic activity. The Journal of Physical Chemistry B. 2005;**109**:20504-20510

[67] Pan C, Takata T, Kumamoto K, Khine Ma SS, Ueda K, Minegishi T, et al. Band engineering of perovskite-type transition metal oxynitrides for photocatalytic overall water splitting. Journal of Materials Chemistry A. 2016; **4**:4544-4552

[68] Xu J, Pan C, Takata T, Domen K. Photocatalytic overall water splitting on the perovskite-type transition metal oxynitride $CaTaO_2N$ under visible light irradiation. Chemical Communications. 2015;**51**:7191-7194

[69] Kibria MG, Nguyen HPT, Cui K, Zhao S, Liu D, Guo H, et al. One-step overall water splitting under visible light using multiband InGaN/GaN nanowire heterostructures. ACS Nano. 2013;**7**: 7886-7893

[70] Liu J, Liu Y, Liu N, Han Y, Zhang X, Huang H, et al. Metal-free efficient photocatalyst for stable visible water splitting via a two-electron pathway. Science (80-). 2015;**347**:970-974

[71] Asai R, Nemoto H, Jia Q, Saito K, Iwase A, Kudo A. A visible light responsive rhodium and antimony-codoped $SrTiO_3$ powdered photocatalyst loaded with an IrO_2 cocatalyst for solar water splitting. Chemical Communications. 2014;**50**:2543-2546

[72] Zhang G, Lan ZA, Lin L, Lin S, Wang X. Overall water splitting by Pt/g-C_3N_4 photocatalysts without using sacrificial agents. Chemical Science. 2016;**7**:3062-3066

[73] Jo WJ, Kang HJ, Kong K-J, Lee YS, Park H, Lee Y, et al. Phase transition-induced band edge engineering of $BiVO_4$ to split pure water under visible light. Proceedings of the National Academy of Sciences. 2015;**112**:13774-13778

[74] Liu H, Yuan J, Shangguan W, Teraoka Y. Visible-light-responding $BiYWO_3$ solid solution for stoichiometric photocatalytic water splitting. Journal of Physical Chemistry C. 2008;**112**:8521-8523

[75] Pan C, Takata T, Domen K. Overall water splitting on the transition-metal oxynitride photocatalyst $LaMg_{1/3}Ta_{2/3}O_2N$ over a large portion of the visible-light spectrum. Chemistry: A European Journal. 2016;**22**:1854-1862

[76] Maeda K, Teramura K, Domen K. Effect of post-calcination on photocatalytic activity of $(Ga_{1-x}Zn_x)(N_{1-x}O_x)$ solid solution for overall water splitting under visible light. Journal of Catalysis. 2008;**254**:198-204

[77] Kato H, Hori M, Konta R, Shimodaira Y, Kudo A. Construction of Z-scheme type heterogeneous photocatalysis systems for water

splitting into H_2 and O_2 under visible light irradiation. Chemistry Letters. 2004;**33**:1348-1349

[78] Abe R, Sayama K, Sugihara H. Development of new photocatalytic water splitting into H_2 and O_2 using two different semiconductor photocatalysts and a shuttle redox mediator IO_3^-/I^-. The Journal of Physical Chemistry. B. 2005;**109**:16052-16061

[79] Abe R, Higashi M, Domen K. Overall water splitting under visible light through a two-step photoexcitation between TaON and WO_3 in the presence of an iodate-iodide shuttle redox mediator. ChemSusChem. 2011;**4**: 228-237

[80] Maeda K, Higashi M, Lu D, Abe R, Domen K. Efficient nonsacrificial water splitting through two-step photoexcitation by visible light using a modified oxynitride as a hydrogen evolution photocatalyst. Journal of the American Chemical Society. 2010;**132**: 5858-5868

[81] Kato H, Sasaki Y, Shirakura N, Kudo A. Synthesis of highly active rhodium-doped $SrTiO_3$ powders in Z-scheme systems for visible-light-driven photocatalytic overall water splitting. Journal of Materials Chemistry A. 2013; **1**:12327-12333

[82] Chen S, Qi Y, Hisatomi T, Ding Q, Asai T, Li Z, et al. Efficient visible-light-driven Z-scheme overall water splitting using a $MgTa_2O_{6-x}Ny$/TaON heterostructure photocatalyst for H_2 evolution. Angewandte Chemie, International Edition. 2015;**54**:8498-8501

[83] Wang Y, Suzuki H, Xie J, Tomita O, Martin DJ, Higashi M, et al. Mimicking natural photosynthesis: Solar to renewable H_2 fuel synthesis by Z-scheme water splitting systems. Chemical Reviews. 2018;**118**:5201-5241

[84] Haumann M, Liebisch P, Muller C, Barra M, Grabolle M, Dau H. Photosynthetic O_2 formation tracked by time-resolved X-ray experiments. Science (80-). 2005;**310**:1019-1021

[85] Leytner S, Hupp JT. Evaluation of the energetics of electron trap states at the nanocrystalline titanium dioxide/aqueous solution interface via time-resolved photoacoustic spectroscopy. Chemical Physics Letters. 2000;**330**:231-236

[86] Wang X, Xu Q, Li M, Shen S, Wang X, Wang Y, et al. Photocatalytic overall water splitting promoted by an α-β phase junction on Ga_2O_3. Angewandte Chemie International Edition. 2012;**51**: 13089-13092

[87] Yoshida Y, Matsuoka M, Moon SC, Mametsuka H, Suzuki E, Anpo M. Photocatalytic decomposition of liquid-water on the Pt-loaded TiO_2 catalysts: Effects of the oxidation states of Pt species on the photocatalytic reactivity and the rate of the back reaction. Research on Chemical Intermediates. 2000;**26**:567-574

[88] Sanap KK, Varma S, Dalavi D, Patil PS, Waghmode SB, Bharadwaj SR. Variation in noble metal morphology and its impact on functioning of hydrogen mitigation catalyst. International Journal of Hydrogen Energy. 2011;**36**:10455-10467

[89] Wang M, Li Z, Wu Y, Ma J, Lu G. Inhibition of hydrogen and oxygen reverse recombination reaction over Pt/TiO_2 by F− ions and its impact on the photocatalytic hydrogen formation. Journal of Catalysis. 2017;**353**:162-170

[90] Berto TF, Sanwald KE, Byers JP, Browning ND, Gutiérrez OY, Lercher JA. Enabling overall water splitting on photocatalysts by CO-covered noble metal co-catalysts. Journal of Physical Chemistry Letters. 2016;**7**:4358-4362

[91] Maeda K, Teramura K, Lu D, Saito N, Inoue Y, Domen K. Roles of Rh/Cr_2O_3 (core/shell) nanoparticles photodeposited on visible-light-responsive $(Ga_{1-x}Zn_x)(N_{1-x}O_x)$ solid solutions in photocatalytic overall water splitting. Journal of Physical Chemistry C. 2007;**111**:7554-7560

[92] Yoshida M, Takanabe K, Maeda K, Ishikawa A, Kubota J, Sakata Y, et al. Role and function of noble-metal/Cr-layer core/shell structure cocatalysts for photocatalytic overall water splitting studied by model electrodes. Journal of Physical Chemistry C. 2009;**113**:10151-10157

[93] Dionigi F, Vesborg PCK, Pedersen T, Hansen O, Dahl S, Xiong A, et al. Suppression of the water splitting back reaction on GaN:ZnO photocatalysts loaded with core/shell cocatalysts, investigated using a μ-reactor. Journal of Catalysis. 2012;**292**:26-31

[94] Nørskov JK, Rossmeisl J, Logadottir A, Lindqvist L, Kitchin JR, Bligaard T, et al. Origin of the overpotential for oxygen reduction at a fuel-cell cathode. The Journal of Physical Chemistry B. 2004;**108**:17886-17892

[95] Takata T, Pan C, Nakabayashi M, Shibata N, Domen K. Fabrication of a core-shell-type photocatalyst via photodeposition of group IV and V transition metal oxyhydroxides: An effective surface modification method for overall water splitting. Journal of the American Chemical Society. 2015;**137**: 9627-9634

[96] Ipek B, Uner D. Artificial photosynthesis from a chemical engineering perspective. In: Najafpour M, editor. Artificial Photosynthesis. IntechOpen; 2012. pp. 13-36

[97] Chen D, Li F, Ray AK. External and internal mass transfer effect on photocatalytic degradation. Catalysis Today. 2001;**66**:475-485

[98] Reilly K, Wilkinson DP, Taghipour F. Photocatalytic water splitting in a fluidized bed system: Computational modeling and experimental studies. Applied Energy. 2018;**222**:423-436

[99] Niu B, Wang X, Wu K, He X, Zhang R. Mesoporous titanium dioxide: Synthesis and applications in photocatalysis, energy and biology. Materials (Basel). 2018;**11**:1-23

[100] Sangle AL, Singh S, Jian J, Bajpe SR, Wang H, Khare N, et al. Very high surface area mesoporous thin films of $SrTiO_3$ grown by pulsed laser deposition and application to efficient photoelectrochemical water splitting. Nano Letters. 2016;**16**:7338-7345

[101] Armenante PM, Kirwan DJ. Mass transfer to microparticles in agitated systems. Chemical Engineering Science. 1989;**44**:2781-2796

[102] Escudero JC, Simarro R, Cervera-March S, Gimenez J. Rate-controlling steps in a three-phase (solid-liquid-gas) photoreactor: A phenomenological approach applied to hydrogen photoproduction using Pt-TiO_2 aqueous suspensions. Chemical Engineering Science. 1989;**44**:583-593

[103] Calderbank PH, Moo-Young MB. The continuous phase heat and mass-transfer properties of dispersions. Chemical Engineering Science. 1961;**16**: 39-54

[104] Uner D, Tapan NA, Özen I, Üner M. Oxygen adsorption on Pt/TiO_2 catalysts. Applied Catalysis A: General. 2003;**251**:225-234

[105] Pinaud BA, Benck JD, Seitz LC, Forman AJ, Chen Z, Deutsch TG, et al. Technical and economic feasibility of centralized facilities for solar hydrogen production via photocatalysis and photoelectrochemistry. Energy & Environmental Science. 2013;**6**:1983-2002

[106] Hisatomi T, Takanabe K, Domen K. Photocatalytic water-splitting reaction from catalytic and kinetic perspectives. Catalysis Letters. 2015;**145**: 95-108

[107] Schröder M, Kailasam K, Borgmeyer J, Neumann M, Thomas A, Schomäcker R, et al. Hydrogen evolution reaction in a large-scale reactor using a carbon nitride photocatalyst under natural sunlight irradiation. Energy Technology. 2015;**3**: 1014-1017

[108] Schneider J, Bahnemann DW. Undesired role of sacrificial reagents in photocatalysis. Journal of Physical Chemistry Letters. 2013;**4**:3479-3483